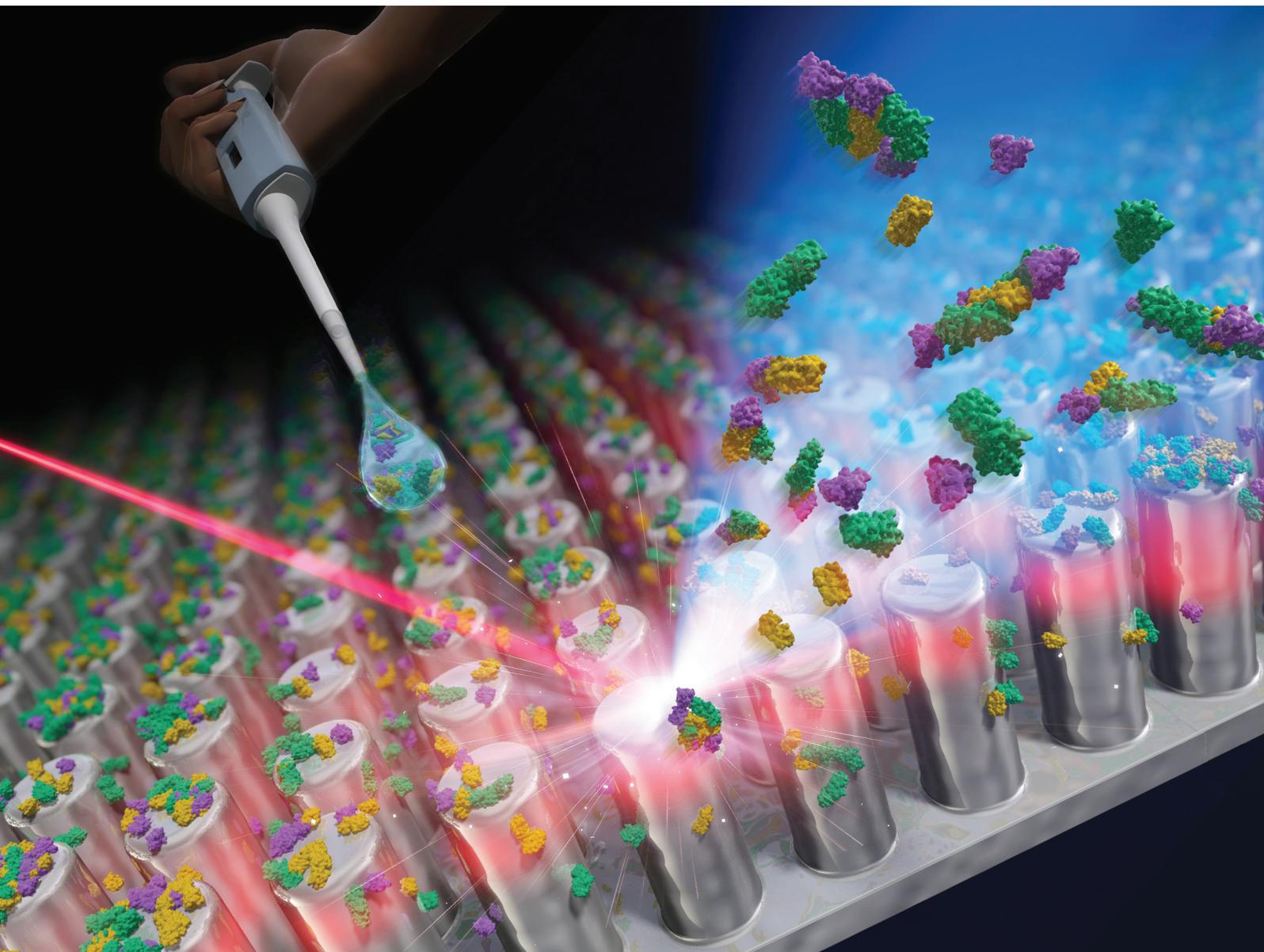# Analyst

ROYAL SOCIETY
OF CHEMISTRY

PAPER
Yuri Yamada, Norihiro Mizoshita *et al.*
TiN nanopillar-enhanced laser desorption and ionization of
various analytes

Check for updates

TiN nanopillar-enhanced laser desorption and ionization of various analytes†

Yuri Yamada, [iD] * Kenichi Yatsugi, [iD] Masakazu Murase [iD] and Norihiro Mizoshita [iD] *

The present paper reports on the use of TiN nanopillars as a robust analytical substrate for laser desorption/ionization mass spectrometry (LDI-MS). TiN nanopillars were fabricated on silicon wafers through the dynamic oblique deposition of titanium, followed by thermal treatment in an ammonia atmosphere. The TiN nanopillars were readily applicable to a simple "dried-droplet" method in the LDI-MS without surface modification or pre-treatment. A broad range of analytes were investigated, including a small drug molecule, a synthetic polymer, sugars, peptides, and proteins. Intact molecular signals were detected with low noise interference and no fragmentation. The developed TiN-nanopillar-based approach extends the applicable mass limit to 150 kDa (immunoglobulin G) and was able to detect trypsinogen (24 kDa) at levels as low as 50 fmol μL^{-1} with adequate shot-to-shot signal reproducibility. In addition, we carried out MS analysis on biomolecule-spiked human blood plasma and a mixture of standard samples to investigate the promise of the TiN nanopillars for clinical research. The experimental observations are validated using electromagnetic and heat-transfer simulations. The TiN nanopillars show a reduced reflection and exhibit surges in the TiN surface temperature upon irradiation with electromagnetic radiation. Localization of thermal energy at the tips of the TiN pillars is likely to be responsible for the superior LDI performance. Our results suggest that the development of nanostructured TiN substrates will contribute to the widespread implementation of nanostructured solid substrates for biomedical and clinical applications with simple processes.

Introduction

Mass spectrometry (MS) is an analytical technique in which specimens are ionized and identified based on their mass-to-charge (m/z) ratios. Matrix-assisted laser desorption/ionization mass spectrometry (MALDI-MS)[1] is a well-established and sophisticated technology to detect various analytes. In MALDI-MS, analyte compounds are crystalized with a UV-absorbing organic matrix that facilitates the desorption and ionization of analytes. Therefore, the matrix/analyte co-crystallization process governs the quality of the acquired mass spectra. Non-uniform analyte/matrix crystallization affords an inhomogeneous sample distribution, leading to "sweet spots".[2] This phenomenon may reduce the shot-to-shot and sample-to-sample reproducibility.

Laser desorption/ionization mass spectrometry (LDI-MS) assisted by nanostructured surfaces of UV-absorbing materials has received much attention as a sister technology of MALDI-MS. The LDI using functional nano surfaces enables avoidance of the abovementioned matrix-related events.[3–17] These kinds of platforms are broadly divided into two types. One uses nanoparticles as the supporting platform, and a variety of materials have been used for this purpose, such as graphite,[4,5] carbon nanotubes,[6] Au nanoparticles,[7] TiO_2 nanoparticles,[8] Pt nanoflowers,[9] and HgTe nanostructures.[10] Analysis using this type of platform is typically called surface assisted LDI-MS (SALDI-MS)[3] or sometimes named nanoparticle-assisted LDI-MS (nano-PALDI-MS).[7] Superior LDI performance has been reported, especially for biomolecules, including proteins with high molecular weights. Chiang *et al.* synthesized HgTe nanoparticles and used them in SALDI-MS in which a high-mass (~150 kDa) protein molecule was successfully ionized.[10] This type of SALDI platform, however, requires careful sample preparation and handling. When a simple "dried-droplet" method is applied to the assembly of nanoparticles, the analyte solution can pass through the spaces between them. To avoid such matter dissipation, it is rec-

Toyota Central R&D Laboratories, Inc., Nagakute, Aichi 480-1192, Japan.
E-mail: e4610@mosk.tytlabs.co.jp, nmizoshita@mosk.tytlabs.co.jp

ommended that the nanoparticles and analyte solutions are mixed beforehand and then pipetted together, which may decrease user-friendliness and hamper qualitative analysis applications. On the other hand, the second type utilizes the nanostructured surfaces of solid substrates. The first example of this type is a chemically etched porous silicon and a set of techniques are named as desorption/ionization on porous silicon mass spectrometry (DIOS-MS).[11] A germanium nanodot chip,[12] nano-imprinted sol-gel film,[13] and silicon nanowire[14] are also applied as the nanostructured substrate for LDI-MS. They are called SALDI-MS as well or occasionally nano-assisted LDI-MS (NALDI-MS). A certain amount of an analytical sample can be applied onto the solid substrate by simply spotting the analyte solution.[11–14] Sample preparation simplicity (user-friendliness) and reproducibility are its major advantages; however, the detectable mass limit of this technique is ~17 kDa.[12] Further effort is required to develop a solid nanostructured LDI platform that enables high-molecular-weight protein ionization.

Despite much pioneering work using various nanoparticles and nanostructured substrates, the LDI mechanism remains contentious because of many factors, including thermal and optical properties, and the chemical interactions between the surface and the analyte affect the LDI phenomenon.[15] Within these properties, thermal transfer of the absorbed laser energy from the supporting surface to the analyte molecules, which should promote analyte vaporization, seems to be a key factor that determines the LDI process.[16] Therefore, substances with lower thermal conductivities are probably more promising for LDI-MS because they suppress the rapid dissipation of the irradiated laser energy. The low thermal conductivities of Pt, Hg, and Te (71.6, 8.34, and 2.35 W m^{-1} K^{-1}, respectively) have been suggested to enable Pt nanoflowers and HgTe nanoparticles to exhibit superior LDI performance.[9,10] However, Pt is a scarce resource, which limits its commercial applications, while the toxicity of HgTe is of concern in terms of potential health effects. In addition, several quasi-molecular ions derived from HgTe-related materials are observed on laser irradiation during the LDI process due to the low melting temperatures of elemental Hg, Te, and HgTe (234, 723, and 943 K, respectively).[10] We recently prepared silicon nanocone arrays and demonstrated the ionization of proteins with molecular weights of up to 17 kDa, which exceeds the mass limit reported using silicon-related nanomaterials.[17] The greatly reduced thermal conductivities of nanoscale pillar and wire geometries[18–20] have been suggested to improve LDI performance. Nanostructured film substrates that satisfy the criteria of efficient laser light absorption as well as reduced thermal conductivity are expected to perform well as convenient LDI-MS substrates for the detection of a wide range of analytes.

In this paper, we develop a user-friendly LDI protocol using titanium nitride (TiN) nanopillar arrays with enhanced LDI performance. The TiN nanopillar arrays function well as robust substrates for the LDI-MS without surface modification or pre-treatment. Just by pipetting a drop of the analyte solution on the surface, TiN nanopillar arrays enable the detection of a broad range of analytes, including high-molecular-weight proteins (immunoglobulin G, IgG), with low background noise and no fragmentation. Because of its broadband light-absorbing properties, TiN can potentially be used in a variety of plasmonic applications, such as solar steam generation,[21,22] and water splitting.[23] The intrinsically low thermal conductivity (16.7 W m^{-1} K^{-1})[24] of TiN is favorable for confining the absorbed thermal energy, which is associated with a surge in the surface temperature. TiN is an abundant and relatively inexpensive material,[25] has a high melting point (>2900 °C),[26] and exhibits good chemical stability.[27] In addition, our approach enables a cost-effective, scalable, and facile manufacturing process. These attractive characteristics are expected to let TiN function well as a UV-absorbing solid LDI-MS platform, as well.

Despite these superior features of TiN, the use of TiN in SALDI-MS has only received limited research attention to date. Schürenberg et al. mixed TiN nanoparticles with a liquid matrix (glycerol) and investigated ionizing proteins and peptides using the obtained suspension.[28] They showed that high-resolution mass spectra could be obtained for peptides with molecular masses of up to 13 kDa. Any protein ions with masses above 30 kDa were not detected by their TiN nanoparticle system; hence further improvement is required. The use of TiN nanopillar arrays is expected to promote the ionization and desorption of protein molecules with high molecular weights due to a surface-temperature surge induced by the nanopillar shape. Electromagnetic and heat-transfer simulations were performed to explore the temperature distribution and LDI behavior of the TiN nanopillar array. The obtained knowledge is helpful to understand the basis of heat transfer in nanopillars, leading to the fabrication of an analytical platform useful in a number of emerging applications.

Experimental

Materials

Granular Ti metal (99.9%; ∅: 10 mm, thickness: 5 mm) was obtained from the Kojundo Chemical Laboratory (Saitama, Japan) and used as a deposition source material. TiN nanoparticles (∅: 50 nm) were purchased from FUJIFILM Wako Pure Chemical (Osaka, Japan). Verapamil (M_w: 454.6) was purchased from Tokyo Chemical Industry (Tokyo, Japan), dipalmitoylphosphatidylcholine (DpPC, M_w: 734.0) was purchased from Hayashi Pure Chemical (Osaka, Japan), and maltoheptaose (M_w: 1153.0) was obtained from Funakoshi (Tokyo, Japan). Trifluoroacetic acid (TFA), acetonitrile (ACN), adenosine (M_w: 267.2), angiotensin I (A1, M_w: 1296.5), polyethylene glycol 4000 (PEG4000), amyloid β-protein (human, 1–40) (Aβ, M_w: 4329.8), and insulin (M_w: 5807) were obtained from FUJIFILM Wako Pure Chemical (Osaka, Japan). β-Cyclodextrin (β-CD, M_w: 1134.9), ubiquitin (M_w: 8560), cytochrome c (M_w: 12 327), myoglobin (M_w: 17 800), trypsinogen (M_w: 24 000), bovine serum albumin (BSA, M_w: 66 000), transferrin (M_w: 79 800), and immunoglobulin G human serum (IgG, M_w: 149 000) were purchased from Sigma Aldrich (Tokyo, Japan). α-Cyano-4-hydroxycinnamic acid (CHCA), peptide calibration

standard (mixture of angiotensin II, angiotensin I, substance P, bombesin, ACTH clip 1–17, ACTH clip 18–39, and somatostatin 28), and protein calibration standard 1 (mixture of insulin, ubiquitin, cytochrome c, and myoglobin) were obtained from Bruker Daltonics (Osaka, Japan). Human plasma was purchased from Cosmo Bio (Tokyo, Japan).

Preparation of TiN nanopillar arrays and TiN thin films

Electron beam (EB) deposition using the oblique angle configuration was used to prepare TiN nanopillar arrays (referred to as "TiN-p") according to our previous report.[29] Two kinds of TiN thin film were prepared. One was prepared with the same EB procedure used to prepare the TiN nanopillars, with the exception that a normal angle configuration without oblique deposition was used (referred to as "TiN-f"). TiN-f was used as the control sample in the LDI-MS experiments. The other was prepared using the radio frequency (RF) sputtering method and was used to acquire optical data and as a reference sample for the heattransfer simulation. Synthesis details and structural characterization data are provided in the ESI.†

LDI-MS using TiN substrates and MALDI-MS

All experiments were conducted using a Bruker Daltonics autoflex maX mass spectrometer equipped with a 355 nm Nd:YAG pulsed laser operating in a positive ion mode at a frequency of 100–200 Hz. The spectrometer was controlled by the flexControl 3.4 software. During sample preparation, the analyte solution was diluted with a mixture of 0.1 vol% aqueous TFA and ACN to final analyte concentrations of 0.001–10.0 pmol μL^{-1}. Mass spectrometry imaging (MSI)[30,31] experiments were performed to evaluate the uniformity of analytes over the whole analysis area and the reproducibility of the detected signal. MSI is commonly used as a label-free technique to study biological tissues but can also be used to investigate the distribution of analyte molecules directly.[32] The MSI and MS using the TiN-x (TiN-f, TiN-p) substrates are referred to as "TiN-x-MSI" and "TiN-x-MS", respectively. Comparative experiments were also carried out using the common MALDI method and TiN nanoparticles as the supporting platform. CHCA was used as the organic matrix for MALDI-MSI. Details of the measurement conditions are presented in the ESI.† Unless otherwise noted, a single-shot MS signal is displayed in the graphs, which may be responsible for the lower signal intensities than those of previous reports in which accumulated shots were often employed.

Preparation of biomolecules-spiked human plasma

Human plasma was pre-treated with ACN according to the previous report.[33] Briefly, an equal amount of ACN was added to the human plasma and the mixture was stored in a refrigerator for 15 min. The supernatant was recovered by centrifugation, followed by dilution at the desired concentration (10–100 times) and spiked with adenosine and amyloid β for LDI-MSI measurements.

Theoretical heat-transfer calculations

The finite-element method (FEM) with the commercial Multiphysics software (version 5.4, COMSOL Inc.) was used to simulate the electromagnetic field and the temperature distribution upon laser irradiation. Pillar arrays of TiN and Si, and a TiN film were simulated to reveal the contribution of the TiN pillar shape to the heat distribution on the surface. High-frequency heating and heat-transfer modules were used along with the electromagnetic heating interface. Further details are provided in electromagnetic and heat-transfer simulation details and in Fig. S1 and Table S2 in the ESI.†
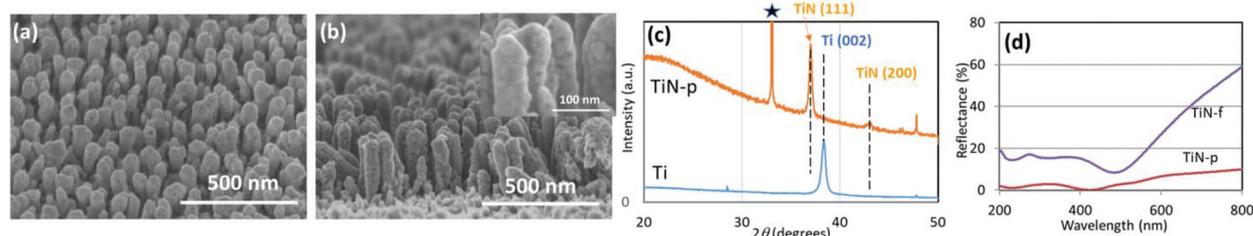
Results and discussion

Characterizing the TiN-p nanostructure

The dynamic oblique deposition of titanium followed by thermal treatment under ammonia was used to prepare TiN nanopillar arrays. In our previous report, TiN nanopillars were prepared on a fused quartz substrate,[29] and the same fabrication method was applied to Si substrates in order to use TiN nanopillar arrays as the LDI-MS platforms. TiN nanopillars were successfully formed even on a silicon substrate, as confirmed by scanning electron microscopy (SEM; Fig. 1a and b). The average height and diameter of the TiN nanopillars were evaluated to be 300 and 60 nm, respectively. The X-ray diffraction (XRD) pattern of TiN-p depicted in Fig. 1c shows peaks derived from TiN's (111) and (200) reflections. The appearance of these peaks and the lack of the Ti (002) peak confirm that Ti pillars have been successfully transformed into TiN. The reflectance spectra of TiN-p and TiN-f are displayed in Fig. 1d; TiN-p exhibits a significantly lower reflectance in the broadband wavelength range compared to TiN-f. TiN-p exhibits a reflectance of less than 2.5% at 355 nm, suggesting that TiN-p uses the irradiated laser energy effectively in the LDI measurements.

It is well known that the formation of nanostructures smaller than the wavelength scale on a film surface leads to reduced light reflection and enhanced light absorption.[34] Fabrication of a subwavelength texture on a silicon surface can lead to broadband antireflection and a dark appearance.[35] The reflective golden color, which is characteristic of bulk TiN[36] (Fig. S2B in the ESI†), was not observed on the TiN-p substrate, which indicates that TiN nanopillars had been uniformly formed throughout the substrate. This simple fabrication strategy can realize the high-throughput manufacture of TiN-p substrates on the centimetre scale (Fig. S4B in the ESI†). We have achieved the scalable fabrication up to 5 cm² substrate size.[37] TiN-f displays the trace metallic color (Fig. S4A in the ESI†) and the reflectance at 355 nm is about 16% (Fig. 1d), which may reflect the surface roughness shown in Fig. S5 in the ESI.†
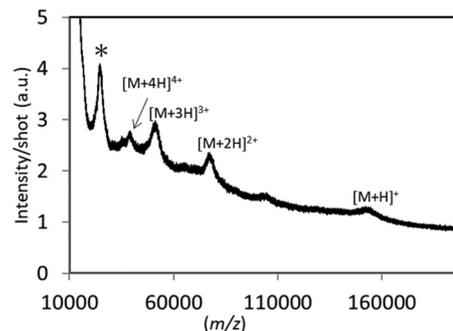
TiN-p-MS for various analyte molecules

There are few reports to date on the ionization of high molecular weight proteins using existing SALDI and the related solid substrate-assisted systems. It is widely accepted that MALDI can easily detect high mass proteins with superior signal sensitivity; however, it is a meaningful challenge to explore new UV-absorbing solid candidates which can spread

Fig. 1 Characterizations of TiN-p. SEM images showing (a) a tilted top view and (b) a cross-sectional view. The inset in (b) shows a magnified image. (c) XRD pattern of TiN-p; the profile of the Ti film is shown for comparison. The peak marked with an asterisk corresponds to Si (002) of the silicon substrate. (d) Reflectance spectra of TiN-f and TiN-p.

mass limit, apart from the established MALDI technique. Various analyte molecules were subjected to LDI with the TiN-p substrate, especially high-mass proteins. Fig. 2 shows the averaged mass spectra obtained for BSA and transferrin using TiN-p-MSI. In both the cases, a singly charged molecular ion as well as multiply charged ions were detected with almost no fragment peaks observed. The corresponding ion maps reveal the presence of peaks of high intensity over the entire detection area, indicating superior uniformity. These results show that TiN-p functions effectively as an analytical substrate for LDI-MS. TiN-p enables the detection of IgG with masses up to 150 000, which, as far as we know, is the detectable mass limit of the SALDI technique.[10] Signals derived from positively charged IgG with low background noise are shown in Fig. 3. Multiply charged ions corresponding to $[M + H]^+$, $[M + 2H]^{2+}$, $[M + 3H]^{3+}$, and $[M + 4H]^{4+}$ were detected at m/z = 150 433, 76 320, 50 105, and 37 620, respectively. Although the intensity
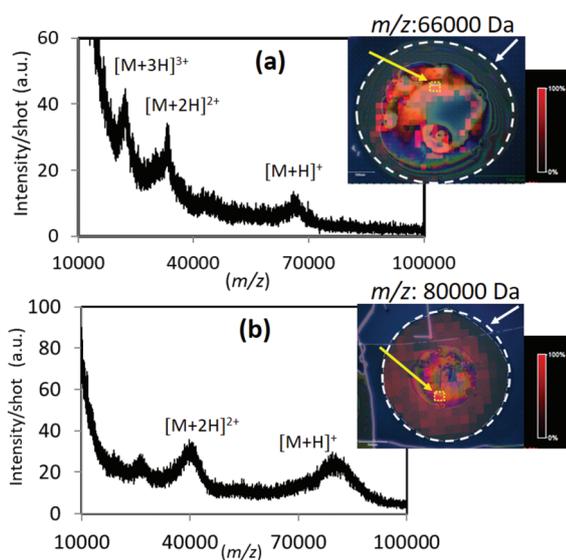

Fig. 3 Averaged mass spectrum obtained for IgG (5 pmol μL^{-1}) on the TiN-p substrate. Spectra acquired over the whole detection area were averaged to provide one spectrum.

Fig. 2 Averaged mass spectra obtained for (a) BSA and (b) transferrin (5 pmol μL^{-1}) on the TiN-p substrate. The insets show the corresponding MS images at m/z: (a) 66 000 Da, and (b) 80 000 Da. The droplet boundaries are indicated by the white dotted lines. Each spectrum was chosen from the area enclosed by the yellow dotted line in the corresponding MS image.

of the detected singly charged molecular ion is not very strong, its spectral feature is similar to that demonstrated by Chiang and co-workers using HgTe nanomaterials.[10] The peak marked with the asterisk corresponds to the quasimolecular ion of two identical light chains of IgG, according to the previous report.[10]
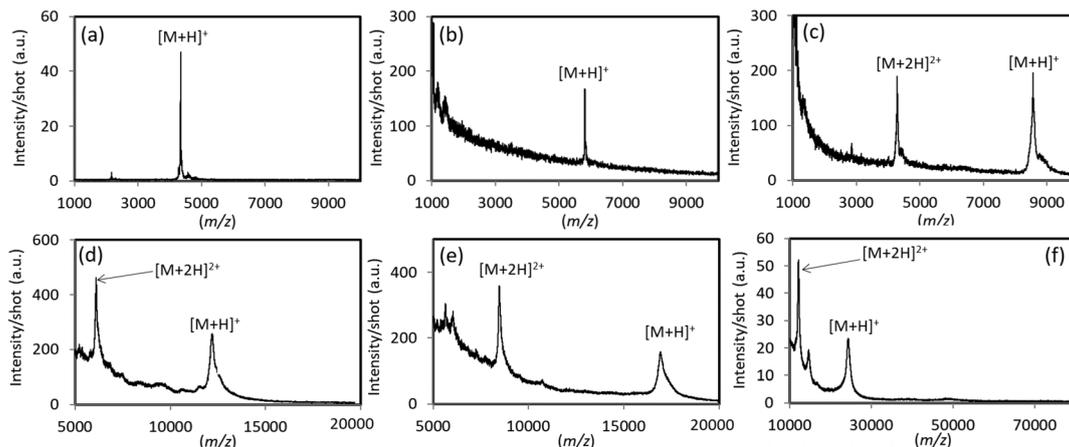
To further demonstrate its utility as an analytical substrate for LDI, TiN-p-MS was used for polypeptides and proteins in the 4000–24 000 Da mass range, and the results are shown in Fig. 4. Peaks derived from protonated molecular ions ($[M + H]^+$) were clearly detected for all target analytes. Multiply charged ions were also detected for ubiquitin, cytochrome c, myoglobin, and trypsinogen (Fig. 4c–f).

TiN-p also facilitates the detection of chemical species with masses below 4000 Da that have been well studied through DIOS[11] and conventional SALDI substrates.[3–10] Mass spectra of a drug (verapamil), a phospholipid (DpPC), sugars (β-CD, maltoheptaose), an oligopeptide (A1), and a polymer (PEG4000) were obtained using TiN-p (Fig. S6 in ESI†). A base fragment ion peak is well known to appear at m/z = 303.0 for verapamil and at m/z = 551.5 for DpPC; no signals were observed at these m/z values by TiN-p-MS (insets of Fig. S6a and S6b†). Taken together, these data and those in Fig. 4 suggest that TiN-p-MS facilitates the detection of intact molecules through soft ionization.

For qualitative comparison purposes, cytochrome c, trypsinogen, and BSA were subjected to MS using TiN-f under the

Fig. 4 Averaged mass spectra of (a) amyloid β (5.0 pmol μL^{-1}), (b) insulin (2.5 pmol μL^{-1}), (c) ubiquitin (5.0 pmol μL^{-1}), (d) cytochrome c (5.0 pmol μL^{-1}), (e) myoglobin (5.0 pmol μL^{-1}), and (f) trypsinogen (5.0 pmol μL^{-1}) obtained using the TiN-p substrate.

identical conditions employed for TiN-p (Fig. S7 in the ESI†). Only broad shoulders corresponding to protonated molecular ions were observed for cytochrome c and trypsinogen, while no signals were observed for BSA, which has a high molecular weight of 66 000 Da. It should be noted that, with the exception of the deposition angle, TiN-f was fabricated using the same methodology used to prepare TiN-p. The obtained results validate that the characteristic TiN nanopillar morphology significantly enhances the performance of TiN as an analytical substrate in LDI-MS.

We further demonstrated the simplicity of MS using the TiN-p substrate by comparing it to SALDI using TiN nanoparticles (Fig. S8 in the ESI†). No signal was observed when A1 was applied to the TiN-nanoparticle substrate in SALDI-MS (Fig. S8B in the ESI†). Pipetting an analytical sample mixture onto these particles led to the propagation of the analyte solution through the cracks between the nanoparticles, which might reduce detection efficiency. Such a phenomenon is peculiar to the particle-based SALDI-MS when the simple "dried-droplet" method is applied, which hinders efficient signal detection. An appropriate procedure, such as nanoparticle/analyte solution pre-mixing or using patterned or hydrophobic substrates, is required to incorporate analyte molecules onto the surfaces of the nanoparticles, which makes the process less convenient. It should be noted that the TiN-p is applied as substrates for the LDI-MS without surface modification or pre-treatment due to its relatively hydrophobic nature (Fig. S9 in the ESI†). Independent of variations of analyte molecules, the same simple sample preparation method (dried-droplet) is used for TiN-p-MS. Just on pipetting a drop of the analyte solution on the surface of the TiN-p, LDI-MS is ready to start. Such a user-friendly method is a considerable advantage of TiN-p-MS.
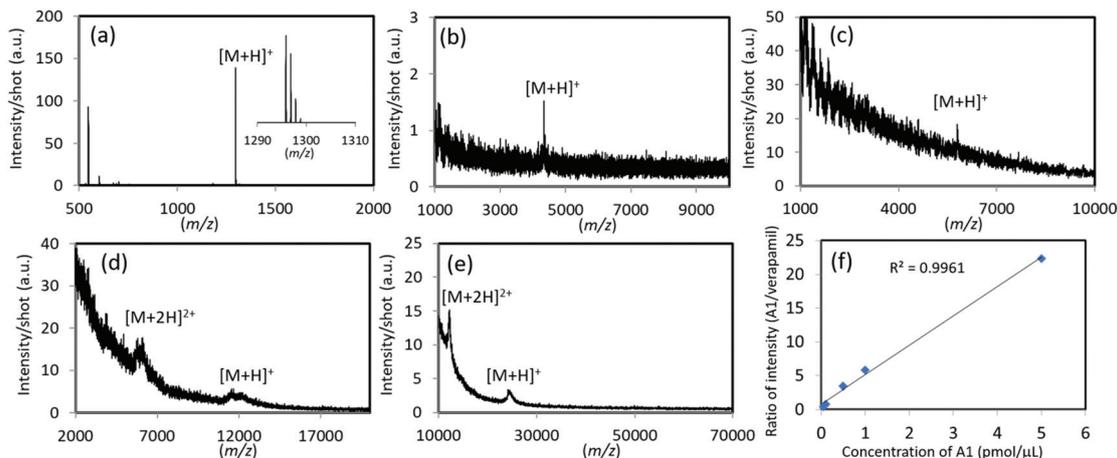
Detecting minute amounts of analyte and evaluating signal reproducibility

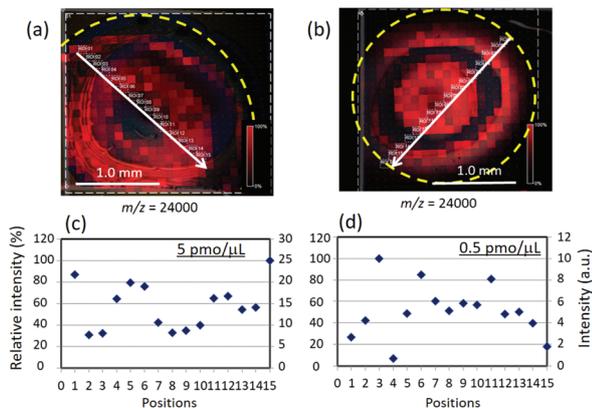The ability of TiN-p-MS to detect minute amounts of analyte was evaluated and the results are shown in Fig. 5a–e.

Using TiN-p, 1 fmol μL^{-1} of A1 was detected with a well resolved isotopic distribution (Fig. 5a); this performance is close to that reported for the germanium nanodot chip (800 fmol).[12] In addition, TiN-p-MS facilitated the detection of trace amounts of analytes with molecular weights over 4000 Da. Limits of detection (LODs) as low as 50 fmol μL^{-1} for amyloid β, 100 fmol μL^{-1} for insulin, 50 fmol μL^{-1} for cytochrome c, and 50 fmol μL^{-1} for trypsinogen were determined (Fig. 5b–e). The quantities of peptides detectable by TiN-p-MS were almost the same as those reported previously. For example, in LDI-MS using Fe$_3$O$_4$/TiO$_2$ nanoparticles, the LODs for A1, insulin, and cytochrome c are 5, 15, and 200 fmol, respectively.[38] Meanwhile, the LOD for trypsinogen (24 kDa) using TiN-p-MS is 50 fmol, which is much lower than those obtained using Fe$_3$O$_4$/TiO$_2$ nanoparticles (8.5 pmol)[38] and Pt nanosponges (50 pmol).[39]

Securing signals quantitatively, reproducibly, and in a high throughput manner is crucial when using LDI-MS as a beneficial tool, such as in clinical diagnosis and the quantitative analysis of pesticide residues. Firstly, we demonstrated the feasibility of using the TiN-p substrate to quantitatively analyze a commonly available peptide molecule (A1). Here, we use an internal standard (verapamil) for improved measurement accuracy.[40] The ratio of the signal intensity of A1 to that of verapamil (0.1 pmol μL^{-1}) is plotted as a function of the concentration of A1 in Fig. 5f, which shows a good linear relationship over the 0.05–5.0 pmol μL^{-1} range, with a coefficient of determination (R^2) of 0.996.

We next investigated signal reproducibility of TiN-p-MSI using a protein molecule with a large molecular weight of 24 kDa (trypsinogen). Fig. 6 shows MS images and the signal-intensity distributions for 5.0 pmol μL^{-1} and 0.5 pmol μL^{-1} trypsinogen. Signal intensities were determined along a randomly selected line in the ion image. Signals were detected over the whole sample area and changing the concentration of trypsinogen did not significantly affect the distribution of analyte molecules (Fig. 6a and b). The average signal intensity

Fig. 5 Sensitivity and signal quantitativity using TiN-p-MSI. (a–e) Averaged mass spectra obtained using the TiN-p substrate for the detection of trace amounts of analytes: (a) A1 (1 fmol μL^{-1}), (b) amyloid β (50 fmol μL^{-1}), (c) insulin (100 fmol μL^{-1}), (d) cytochrome c (50 fmol μL^{-1}), and (e) trypsinogen (50 fmol μL^{-1}). Inset in (a) displays the isotopic distribution of A1. (f) Relative intensity as a function of A1 concentration obtained using TiN-p-MSI. The coefficient of determination (R^2) is shown in the graph. Each spectrum is the accumulation of 100 shots and five spectra at different points were averaged to provide each point. A low amount of citric acid (0.004 $\mu mol\ \mu L^{-1}$) was used.

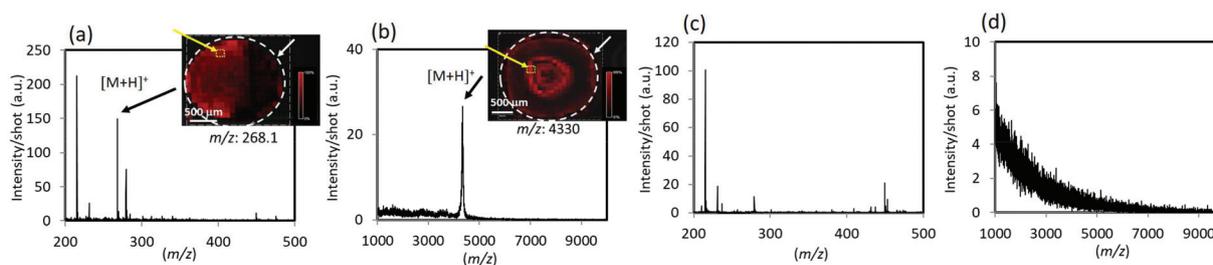**Fig. 6** TiN-p-MSI for trypsinogen (m/z = 24 000) of (a and c) 5.0 pmol μL^{-1}, and (b, d) 0.5 pmol μL^{-1}. (a and b) MS ion images. The droplet boundaries are indicated by yellow dotted lines. (c and d) Variations in the relative signal intensities of trypsinogen (left axes) and signal intensity (right axes) obtained from the MS ion images in the same column. The data were collected from different sample spots along the white arrows shown in the corresponding MS image, where the highest signal intensity was set to 100%. Numbers on the horizontal axes correspond to measurement points along the white arrows, from the starting point to the terminal, as depicted in the MS images. A S/N ratio >3 was used as the signal detection criterion.

and the standard deviation along the white lines in the MS images are 14.1, 5.16 for 5.0 pmol μL^{-1} and 5.02, 2.30 for 0.5 pmol μL^{-1}, respectively. The results indicate the adequate signal reproducibility of TiN-p-MSI. Over the years, much work has demonstrated that the SALDI approach improves analyte homogeneity as well as signal reproducibility; however, the target molecules have been limited to peptides and drugs with relatively low molecular weights.[9,40] The same experiments

were conducted on MALDI-MS and a more variable intensity distribution was observed (Fig. S10 in ESI†).

Detection of target molecules from human blood plasma and mixtures

In addition to the LDI-MS of individual analyte molecules, detection of target signals from the real bio-related samples or mixed compounds is addressed in this section to demonstrate the feasibility of the TiN-p-MS. Fig. 7 compares the mass spectra of unspiked supernatant human plasma and that spiked with adenosine or amyloid β. Adenosine is a type of nucleoside, which is essential for all life.[41] Amyloid-β peptide plays an important role in the development of Alzheimer's disease.[42] Several ionic species derived from human plasma were detected in the low m/z ranges (Fig. 7c). The protonated adducts of adenosine and amyloid-β were clearly detected at m/z of 268.1 and 4330 in the mass spectra of the supernatant plasma mixtures, respectively (Fig. 7a and b). The MS ion images (inset) indicate that signals were detectable throughout the sample area even when the complex samples were used. The observed reproducibility enables us to determine the calibration curves of adenosine in the supernatant human plasma. A good linear relationship was confirmed for both pure adenosine and adenosine added in the supernatant human plasma (Fig. S11 in the ESI†). We further performed signal detection of mixed peptides and proteins (Fig. S12 in the ESI†). Well-resolved mass spectra were obtained from mixture solutions and all peptides and proteins present in the analytical solution are observed as [M + H]$^+$ peaks with a high S/N ratio. The results demonstrate that TiN-p-MS facilitates the simultaneous detection of complexed or multiple molecules and highlights its potential use in applications, such as the analysis of complex biological samples. We briefly investigated the salt tolerance and the durability of the TiN-p substrate

Fig. 7 Averaged mass spectra obtained of (a) adenosine-spiked, (b) amyloid β-spiked, and (c and d) unspiked supernatant human plasma obtained using TiN-p substrate. Insets are the corresponding MS-images at *m/z* (a) 268.1, and (b) 4330, respectively. The droplet boundaries are outlined in white dotted lines. Each spectrum is chosen from the area outlined in yellow dotted lines in the MS-image. The concentrations of analyte were (a) 10.0 pmol μL^{-1}, and (b) 5.0 pmol μL^{-1}.

(Fig. S13 and S14 in the ESI†). The signal intensity of protonated A1 decreased under a high-salt concentration, which we regard as a challenge for future work (Fig. S13 in the ESI†). Meanwhile, durability of the TiN-p substrate upon laser irradiation is high due to the intrinsic nature of TiN (Fig. S14 in the ESI†).
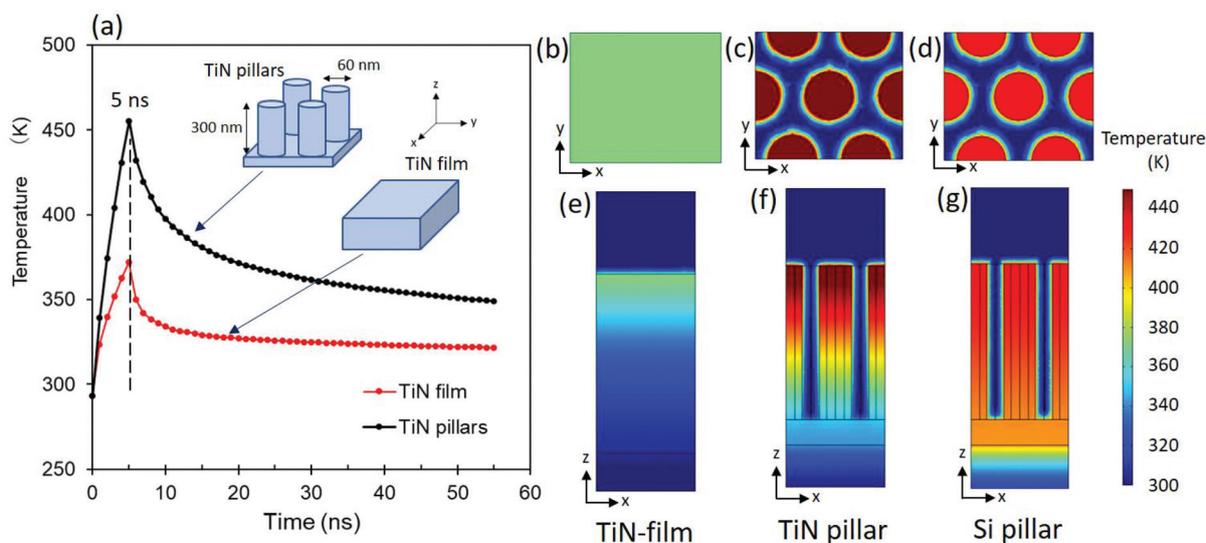
Theoretical explanation of heattransfer of TiN-p substrate

In this section, we used FEM simulations to explain the improved performance of TiN-p as an analytical substrate for matrix-free LDI-MS through a theoretical approach. To simplify these simulations, we employed cylindrical pillars (TiN pillars) and a flat surface (TiN film) as models of TiN-p and TiN-f, respectively (Fig. S1 in the ESI†). In addition, model Si pillars, which are commonly used as substrates in SALDI-MS, such as DIOS (porous silicon), were also simulated.[11]

The electromagnetic field was first simulated to obtain the optical properties of the TiN film and TiN pillars at λ = 355 nm (Fig. S15 in the ESI†). The reflectance, absorbance, and trans-

mittance of the TiN film were calculated to be 22%, 78%, and 0%, respectively. The reflectance of the TiN pillars was calculated to be significantly lower, at 3%, and enhanced absorption (95%) was observed; these values are in good agreement with the measured values of reflectance and transmittance (Fig. 1d and S2 in the ESI†). The observed rise in the transmittance of TiN-p (2%, see Fig. S15 in the ESI†) is ascribable to a reduction in optical loss due to suppressed reflection and the smaller volume of the light-absorbing TiN substance.

Fig. 8 provides a summary of heat transfer based on the electromagnetic simulations. Fig. 8a shows that both the TiN film and the TiN pillars exhibit a spike in temperature immediately after electromagnetic irradiation (5 ns). After being irradiated for 5 ns with the electromagnetic wave, the temperature distribution of surface of the TiN film is quite uniform (370 K) in the *xy* plane (Fig. 8b). Only a small change in temperature was observed along the *z* axis for the TiN film (Fig. 8e). On the other hand, the TiN pillars show localized thermal energy; the temperature at the tips of the TiN pillars

Fig. 8 Theoretical heat-transfer modeling. (a) Temperatures of the top surfaces of the TiN film and the TiN pillars as functions of time after irradiation with an electromagnetic wave (355 nm, 5 ns). (b–g) Temperature distributions in the (b–d) *xy* and (e–g) *xz* planes after irradiating (b, e) the TiN film, (c, f) the TiN pillar, and (d, g) the Si pillar for 5 ns.

was remarkably higher (>450 K) compared to that observed for the TiN film (Fig. 8b and c). The tips of the TiN pillars show the highest temperature and a large temperature gradient is evident in moving from the top to the bottom of each pillar (z direction) (Fig. 8f), which indicates that heat is confined to the tips of the TiN pillars. The characteristics of TiN pillars are highlighted when compared to the simulated result for Si pillars. Heat transfer in the model Si pillars with the same dimensions as the TiN pillars was simulated under identical conditions to those used to simulate the TiN pillars. The Si pillars exhibited only a small temperature difference along the z axis after irradiation for 5 ns, indicating that heat is promptly dissipated in the Si substrate (Fig. 8g). The intrinsic lower thermal conductivity of the TiN pillar (16.7 W m^{-1} K^{-1}, Table S2†) compared to the Si pillar (160 W m^{-1} K^{-1}, Table S2†) is responsible to the effective heat confinement for TiN pillars, which may lead to enhanced LDI performance when compared to that previously reported for Si-related substrates.

It has been hypothesized that the pillar or wire shape enables to confine heat effectively, leading to the positive effect on the LDI performance.[43,44] In this study, heat-transfer simulations clearly reproduced the observed confinement of heat generated by the localization of light energy at the tips of the TiN pillars. The present results should be used to further improve LDI performance. We are continuing in making progress in the development of TiN-p-MS for biomedical and clinical applications.

Conclusions

We demonstrated that TiN nanopillars prepared by the dynamic oblique deposition of titanium followed by thermal treatment in ammonia vapor show excellent functionality as a robust analytical substrate for LDI-MS. The TiN nanopillars function as the analytical substrate without surface modification or pre-treatments. Whatever the types and molecular weights of analytical molecules, the simple "dried-droplet" method can be applied for LDI measurements, which is advantageous to provide a convenient analytical method. The same "dried-droplet" method is applicable for mass spectrometry imaging measurements as well. A wide range of analytes, including a drug, sugars, and bio-related materials were detected with low levels of noise interference. The detectable mass limit using this approach is 150 kDa (IgG), which is comparable to the best result previously reported using HgTe nanoparticles. Proteins and peptides were detected at concentrations of several tens of femtomoles, and a detection limit of 50 fmol μL^{-1} was accomplished for trypsinogen (24 kDa); this performance is similar to or better than that reported for other SALDI techniques. A comparative study revealed that the TiN nanopillar substrate exhibited improved shot-to-shot reproducibility for the detection of trypsinogen. In addition, the TiN nanopillar substrate performed simultaneous detection of multiple biomolecules in human blood plasma. The superior

LDI performance of the TiN substrate was validated by electromagnetic and heat-transfer simulations. The reduction in light reflection due to the pillar shape is well reproduced by the simulated electromagnetic data. In addition, the localization of heat on the tips of the TiN pillars was demonstrated in the heat-transfer simulation, which suggests that synergism between the intrinsically high light-absorption properties of TiN, reduced light reflection, and the heat confinement effect leads to a significant enhancement in LDI performance. This study revealed that TiN nanopillar arrays can feasibly be used as robust analytical substrates for LDI-MS while providing basic insights into the thermal distributions in nanostructures. We believe that the results reported herein will lead to optimal substrate designs for effective thermal management during LDI.

Author contributions

The manuscript was written through contributions of all authors. All authors have given approval to the final version of the manuscript.

Conflicts of interest

There are no conflicts to declare.

Acknowledgements

Notes and references

1 M. Karas and F. Hillenkamp, *Anal. Chem.*, 1988, **60**, 2299–2301.
2 G. Stübiger and O. Belgacem, *Anal. Chem.*, 2007, **79**, 3206–3213.
3 C.-K. Chiang, W.-T. Chen and H.-T. Chang, *Chem. Soc. Rev.*, 2011, **40**, 1269–1281.
4 J. Wang, Q. Liu, Y. Liang and G. Jiang, *Anal. Bioanal. Chem.*, 2016, **408**, 2861–2873.
5 J. Sunner, E. Dratz and Y.-C. Chen, *Anal. Chem.*, 1995, **67**, 4335–4342.
6 S. Y. Xu, Y. F. Li, H. F. Zou, J. S. Qiu, Z. Guo and B. C. Guo, *Anal. Chem.*, 2003, **75**, 6191–6195.
7 S. Taira, I. Osaka, S. Shimma, D. Kaneko, T. Hiroki, Y. Kawamura-Konishi and Y. Ichiyanagi, *Analyst*, 2012, **137**, 2006–2010.
8 M. Lu, X. Yang, Y. Yang, P. Qin, X. Wu and Z. Cai, *Nanomaterials*, 2017, **7**, 87.

9   H. Kawasaki, T. Yonezawa, T. Watanabe and R. Arakawa, *J. Phys. Chem. C*, 2007, **111**, 16278–16283.

10 C.-K. Chiang, Z. Yang, Y.-W. Lin, W.-T. Chen, H.-J. Lin and H.-T. Chang, *Anal. Chem.*, 2010, **82**, 4543–4550.

11 J. Wei, J. M. Buriak and G. Siuzdak, *Nature*, 1999, **399**, 243–246.

12 T. Seino, H. Sato, A. Yamamoto, A. Nemoto, M. Torimura and H. Tao, *Anal. Chem.*, 2007, **79**, 4827–4832.

13 N. Mizoshita, Y. Yamada, M. Murase, Y. Goto and S. Inagaki, *Nanoscale*, 2020, **12**, 21146–21154.

14 G. Piret, D. Kim, H. Drobecq, Y. Coffinier, O. Melnyk, P. Schmuki and R. Boukherroub, *Analyst*, 2012, **137**, 3058–3063.

15 H.-W. Tang, K.-M. Ng, W. Lu and C.-M. Che, *Anal. Chem.*, 2009, **81**, 4720–4729.

16 J. J. Zhu, X. Meng, C. Zhang, J. Bian, Z.D. Lu, Y. Liu and W. H. Zhang, *Phys. Chem. Chem. Phys.*, 2018, **20**, 3424–3429.

17 Y. Yamada, H. Iizuka and N. Mizoshita, *ACS Appl. Nano Mater.*, 2020, **3**, 4231–4240.

18 J. Guo, B. Wen, R. Melnik, S. Yao and T. Li, *Physica E Low Dimens. Syst. Nanostruct.*, 2010, **43**, 155–160.

19 D. Li, Y. Wu, P. Kim, L. Shi, P. Yang and A. Majumdar, *Appl. Phys. Lett.*, 2003, **83**, 2934–2936.

20 X. Chen, T. Wang, L. Lin, F. Wo, Y. Liu, X. Liang, H. Ye and J. Wu, *ACS Appl. Mater. Interfaces*, 2018, **10**, 14389–14398.

21 S. Ishii, R. P. Sugavaneshwar and T. Nagao, *J. Phys. Chem. C*, 2016, **120**, 2343–2348.

22 M. Kaur, S. Ishii, S. L. Shinde and T. Nagao, *Adv. Sustain. Syst.*, 2019, **3**, 1800112.

23 A. Naldoni, U. Guler, Z. Wang, M. Marelli, F. Malara, X. Meng, L. V. Besteiro, A. O. Govorov, A. V. Kildishev, A. Boltasseva and V. M. Shalaev, *Adv. Opt. Mater.*, 2017, **5**, 1601031.

24 S. G. Choi, T.-J. Ha, B.-G. Yu, S. Shin, H. H. Cho and H.-H. Park, *Thin Solid Films*, 2007, **516**, 212–215.

25 N. Venugopal, V. S. Gerasimov, A. E. Ershov, S. V. Karpov and S. P. Polyutov, *Opt. Mater.*, 2017, **72**, 397–402.

26 J. A. Briggs, G. V. Naik, Y. Zhao, T. A. Petach, K. Sahasrabuddhe, D. Goldhaber-Gordon, D. N. A. Melosh and J. A. Dionne, *Appl. Phys. Lett.*, 2017, **110**, 101901.

27 G. V. Naik, V. M. Shalaev and A. Boltasseva, *Adv. Mater.*, 2013, **25**, 3264–3294.

28 M. Schürenberg, K. Dreisewerd and F. Hillenkamp, *Anal. Chem.*, 1999, **71**, 221–229.

29 K. Yatsugi and K. Nishikawa, *Nanotechnology*, 2019, **30**, 335705.

30 R. M. Caprioli, T. B. Farmer and J. Gile, *Anal. Chem.*, 1997, **69**, 4751–4760.

31 D. S. Cornett, M. L. Reyzer, P. Chaurand and R. M. Caprioli, *Nat. Methods*, 2007, **4**, 828–833.

32 H. Qiao, G. Piyadasa, V. Spicer and W. Ens, *Int. J. Mass Spectrom.*, 2009, **281**, 41–51.

33 A. Hamdi, I. S. Hosu, A. Addad, R. Hartkoorn, H. Drobecq, O. Melnyk, H. Ezzaouia, R. Boukherroub and Y. Coffinier, *Talanta*, 2017, **171**, 101–107.

34 F. Flory, L. Escoubas and G. Berginc, *J. Nanophotonics*, 2011, **5**, 052502.

35 X. Liu, P. R. Coxon, M. Peters, B. Hoex, J. M. Cole and D. J. Fray, *Energy Environ. Sci.*, 2014, **7**, 3223–3263.

36 W. P. Guo, R. Mishra, C. W. Cheng, B.-H. Wu, L.-J. Chen, M.-T. Lin and S. Gwo, *ACS Photonics*, 2019, **6**, 1848–1854.

37 K. Nishikawa and K. Yatsugi, *Nanotechnology*, 2021, **32**, 155404.

38 C.-T. Chen and Y.-C. Chen, *Anal. Chem.*, 2005, **77**, 5912–5919.

39 C. K. Chiang, N. C. Chiang, Z. H. Lin, G. Y. Lan, Y. W. Lin and H. T. Chang, *J. Am. Soc. Mass Spectrom.*, 2010, **21**, 1204–1207.

40 T.-R. Kuo, J.-S. Chen, Y.-C. Chiu, C.-Y. Tsai, C.-C. Hu and C.-C. Chen, *Anal. Chim. Acta*, 2011, **699**, 81–86.

41 F. Ding, Y. Qian, Z. A. Deng, J. T. Zhang, Y. C. Zhou, L. Yang, F. Y. Wang, J. P. Wang, Z. H. Zhou and J. L. Shen, *Nanoscale*, 2018, **10**, 22044–22054.

42 M. P. Murphy and H. LeVine 3rd, *J. Alzheimer's Dis.*, 2010, **19**, 311–323.

43 E. P. Go, J. V. Apon, G. Luo, A. Saghatelian, R. H. Daniels, V. Sahi, R. Dubrow, B. F. Cravatt, A. Vertes and G. Siuzdak, *Anal. Chem.*, 2005, **77**, 1641–1646.

44 Y. Coffinier, S. Szunerits, H. Drobecq, O. Melnyk and R. Boukherroub, *Nanoscale*, 2012, **4**, 231–238.